Multisize Electrode Field-of-View

Validation by High Resolution Gadolinium-Enhanced Cardiac Magnetic Resonance

Omara, Sharif; Glashan, Claire A.; Tofig, Bawer J.; Leenknegt, Lore; Dierckx, Hans; Panfilov, Alexander V.; Beukers, H; Tao, Qian; van der Geest, Rob J.; More Authors

DOI
10.1016/j.jacep.2023.12.003

Publication date
2024

Document Version
Final published version

Published in
JACC: Clinical Electrophysiology

JACC: CLINICAL ELECTROPHYSIOLOGY VOL. 10, NO. 4, 2024

ORIGINAL RESEARCH

VENTRICULAR ARRHYTHMIAS - CATHETER ABLATION

Multisize Electrode Field-of-View

Validation by High Resolution Gadolinium-Enhanced Cardiac Magnetic Resonance

Sharif Omara, MBBS,[a,b] Claire A. Glashan, MD,[a,b] Bawer J. Tofig, MD,[a,c] Lore Leenknegt, MSc,[d] Hans Dierckx, PhD,[d] Alexander V. Panfilov, PhD,[e] Hans K.C. Beukers, MD,[b] Michiel H. van Waasbergen, BSc,[b] Qian Tao, PhD,[f] William G. Stevenson, MD,[g] Jens C. Nielsen, MD, PhD,[a,c] Peter Lukac, MD, PhD,[a,c] Steen B. Kristiansen, MD, PhD,[a,c] Rob J. van der Geest, PhD,[h] Katja Zeppenfeld, MD, PhD[a,b,c]

ABSTRACT

BACKGROUND Voltage mapping to detect ventricular scar is important for guiding catheter ablation, but the field-of-view of unipolar, bipolar, conventional, and microelectrodes as it relates to the extent of viable myocardium (VM) is not well defined.

OBJECTIVES The purpose of this study was to evaluate electroanatomic voltage-mapping (EAVM) with different-size electrodes for identifying VM, validated against high-resolution ex-vivo cardiac magnetic resonance (HR-LGE-CMR).

METHODS A total of 9 swine with early-reperfusion myocardial infarction were mapped with the QDOT microcatheter. HR-LGE-CMR (0.3-mm slices) were merged with EAVM. At each EAVM point, the underlying VM in multisize transmural cylinders and spheres was quantified from ex vivo CMR and related to unipolar and bipolar voltages recorded from conventional and microelectrodes.

RESULTS In each swine, 220 mapping points (Q1, Q3: 216, 260 mapping points) were collected. Infarcts were heterogeneous and nontransmural. Unipolar and bipolar voltage increased with VM volumes from >175 mm^3 up to >525 mm^3 (equivalent to a 5-mm radius cylinder with height >6.69 mm). VM volumes in subendocardial cylinders with 1- or 3-mm depth correlated poorly with all voltages. Unipolar voltages recorded with conventional and microelectrodes were similar (difference 0.17 ± 2.66 mV) and correlated best to VM within a sphere of radius 10 and 8 mm, respectively. Distance-weighting did not improve the correlation.

CONCLUSIONS Voltage increases with transmural volume of VM but correlates poorly with small amounts of VM, which limits EAVM in defining heterogeneous scar. Microelectrodes cannot distinguish thin from thick areas of subendocardial VM. The field-of-view for unipolar recordings for microelectrodes and conventional electrodes appears to be 8 to 10 mm, respectively, and unexpectedly similar. (J Am Coll Cardiol EP 2024;10:637-650) © 2024 The Authors. Published by Elsevier on behalf of the American College of Cardiology Foundation. This is an open access article under the CC BY license (http://creativecommons.org/licenses/by/4.0/).

From the [a]Willem Einthoven Center for Cardiac Arrhythmia Research and Management, Leiden, the Netherlands, and Aarhus, Denmark; [b]Department of Cardiology, Leiden University Medical Center, Leiden, the Netherlands; [c]Department of Cardiology, Aarhus University Hospital, Aarhus, Denmark; [d]Department of Mathematics, KU Leuven campus Kortrijk, Kortrijk, Belgium; [e]Department of Physics and Astronomy, Ghent University, Ghent, Belgium; [f]Department of Imaging Physics, Delft University of Technology, Delft, the Netherlands; [g]Division of Cardiovascular Medicine, Vanderbilt University Medical Center, Nashville, Tennessee, USA; and the [h]Department of Radiology, Division of Image Processing, Leiden University Medical Center, Leiden, the Netherlands.

The authors attest they are in compliance with human studies committees and animal welfare regulations of the authors' institutions and Food and Drug Administration guidelines, including patient consent where appropriate. For more information, visit the Author Center.

Manuscript received June 1, 2023; revised manuscript received December 1, 2023, accepted December 4, 2023.

ISSN 2405-500X https://doi.org/10.1016/j.jacep.2023.12.003

JACC: CLINICAL ELECTROPHYSIOLOGY VOL. 10, NO. 4, 2024
APRIL 2024:637–650

ABBREVIATIONS AND ACRONYMS

BV_c = conventional bipolar voltage

BV_μ = micro bipolar voltage

EAVM = electro-anatomical voltage mapping

EGM = electrogram

LGE-CMR = late-gadolinium enhancement cardiac magnetic resonance

MI = myocardial infarction

UV_c = conventional unipolar voltage

UV_μ = micro unipolar voltage

VM = viable myocardium

Myocardial infarction (MI) results in scars with diverse distributions and degrees of transmurality, depending on the time-to-reperfusion and the anatomy of the underlying (affected) arterial supply.[1-4] Early reperfusion of MI is known to reduce scar transmurality and local wall thinning.[5,6] A heterogeneous mix of viable myocardium (VM) and fibrosis is an important substrate for re-entrant ventricular tachycardia postinfarction and in nonischemic cardiomyopathy.

Identification of ventricular scars with catheter mapping relies on delimiting low-voltage areas using electroanatomic voltage mapping (EAVM) and is well established.[7] The commonly used voltage cutoffs for scar core and border zone (<0.5 and <1.5 mV) are specific for the presence of some degree of fibrosis and are reliably present when fibrosis is transmural. However, these voltage cutoffs do not reflect the extent and heterogeneity of fibrosis in regions of nontransmural scar as identified by histology or late gadolinium-enhanced (LGE) cardiac magnetic resonance (CMR) imaging.[8] Better characterization of potential arrhythmia substrate from voltage maps is desirable, and a combination of unipolar and bipolar mapping and the availability of catheters with conventional and microelectrodes is of interest for this purpose.

Electrode sizes and configurations for EAVM have evolved over time. Unipolar electrograms (EGMs) are recorded and bipolar EGMs constructed from 2 unipolar recordings. Decreasing the size and interelectrode spacing of electrodes for bipolar EGM recordings results in better cancellation of voltages generated by remote VM and thereby limits the field-of-view. The enhanced spatial and temporal resolution in the nearfield of small electrode catheters compared with larger electrode conventional catheters has the potential to improve transmural tissue characterization by voltage mapping.[9-12] However, the true field-of-view, defined as the distance within which VM affects local EGM amplitudes recorded from different size electrodes, is unclear. The field-of-view is 3-dimensional (3D), yet previous studies have (to the authors' knowledge) only correlated EAVM

FIGURE 1 Schematic Representation of the Qdot Catheter

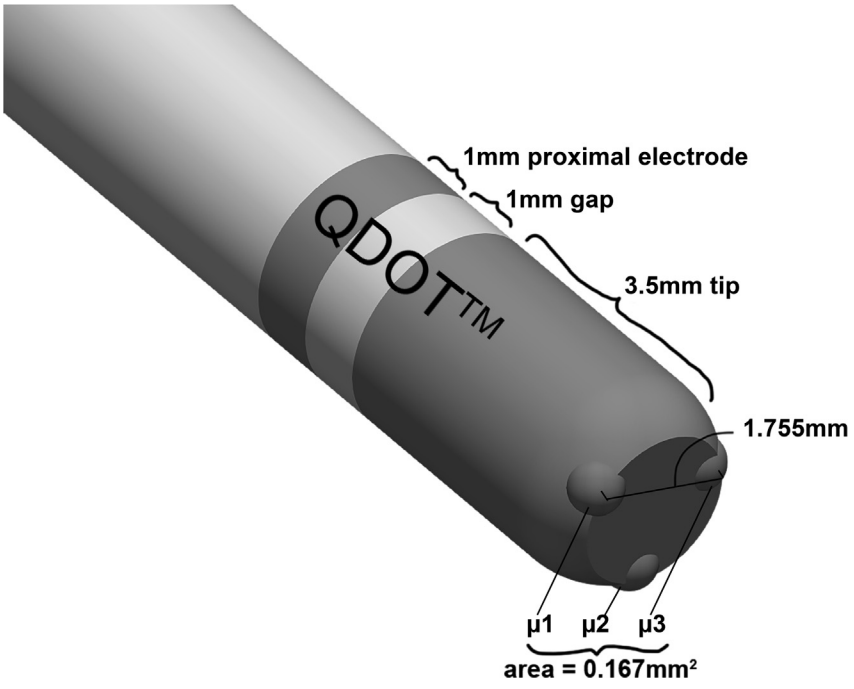

The Qdot 3.5-mm tip electrode incorporates 3 microelectrodes (surface area 0.167 mm^2, interelectrode distance [minimal] 1.349 mm and [center-to-center] 1.755 mm, angle between microbipoles 60°), recording 3 microbipolar electrograms perpendicular to the vector of the BV_c measured between M1 (3.5-mm tip) and M2 (1-mm ring, interelectrode distance [minimal] 1 mm and [center-to-center] 3.25 mm).[9]

FIGURE 2 High Resolution Ex-Vivo Late-Gadolinium Enhanced Cardiac Magnetic Resonance Scar Patterns

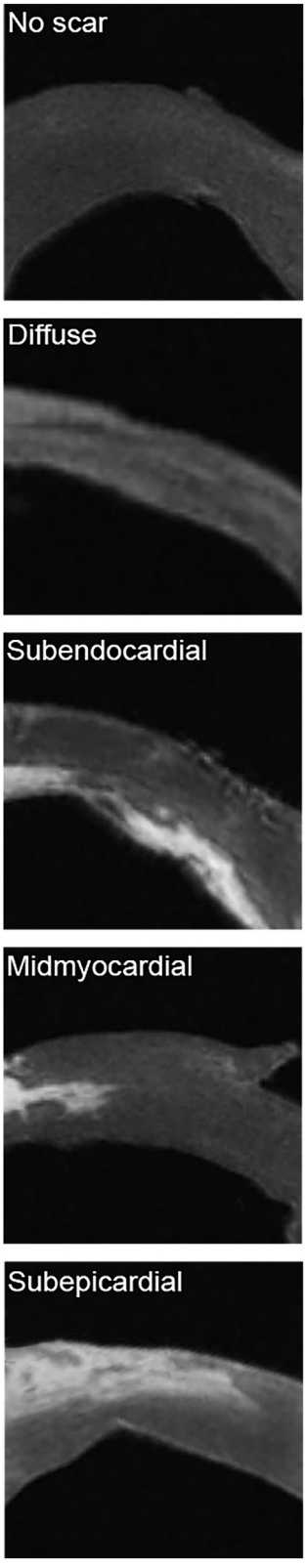

Continued in the next column

with 2-dimensional (2D) parameters such as wall thickness (WT), histology, or 2D-CMR slices.[9,11-13] Knowing the true field-of-view is particularly important for the delineation of nontransmural scars and nonischemic fibrosis, which often affects midmyocardial and subepicardial layers in regions with preserved WT.

The aim of this study is to evaluate the field-of-view of unipolar and bipolar recordings from (narrow-spaced) microelectrodes (micro unipolar voltage [UV_{μ}] and micro bipolar voltage [BV_{μ}]) and conventional electrodes (conventional unipolar voltage [UV_{c}] and conventional bipolar voltage [BV_{c}]) by integrating high-resolution LGE-CMR with EAVM data. For this purpose, we propose a novel method to calculate volumes of VM derived from 3D ex vivo high-resolution LGE-CMR data in a porcine reperfusion infarction model with heterogeneous scar.

METHODS

ANIMAL MODEL. The study was approved by the Danish Animal Experiments Inspectorate (study license number 2017-15-0201-01259). As previously described,[13] in 9 domestic Danish swine (67 ± 2 kg), an anteroseptal MI was induced by 65 minutes of percutaneous coronary balloon occlusion of the left anterior descending (LAD) artery after the second diagonal branch. All animals survived until electrophysiological procedure (84 ± 11 days after infarction).

ELECTROANATOMIC MAPPING. Detailed endocardial EAVM of the left ventricle was performed during sinus rhythm or atrial pacing (in case of sinus bradycardia) using the QDot Microcatheter (**Figure 1**) and CARTO 3 version 6.0 (Biosense Webster). The details of the mapping protocol are provided in the Supplemental Appendix (**Figure 1**).

The BV_{c} value is generated by subtracting the proximal ring electrode signal from the distal tip electrode signal. At each mapping point, the highest of the 3 UV_{μ} and BV_{μ} measurements was determined

FIGURE 2 Continued

The American Heart Association 17-segment model was used when quantifying scar patterns. The predominant scar type in each segment for each heart was determined and the distribution quantified according to the number of segments with a specific pattern. The scar patterns were predefined as 5 groups: transmural, subendocardial, intramural, subepicardial, and diffuse. Diffuse scar was defined as viable myocardium interspersed with scar throughout at least 50% of the transmurality.

FIGURE 3 **Integration of In-Vivo Mapping Data With Ex-Vivo High Resolution LGE-CMR**

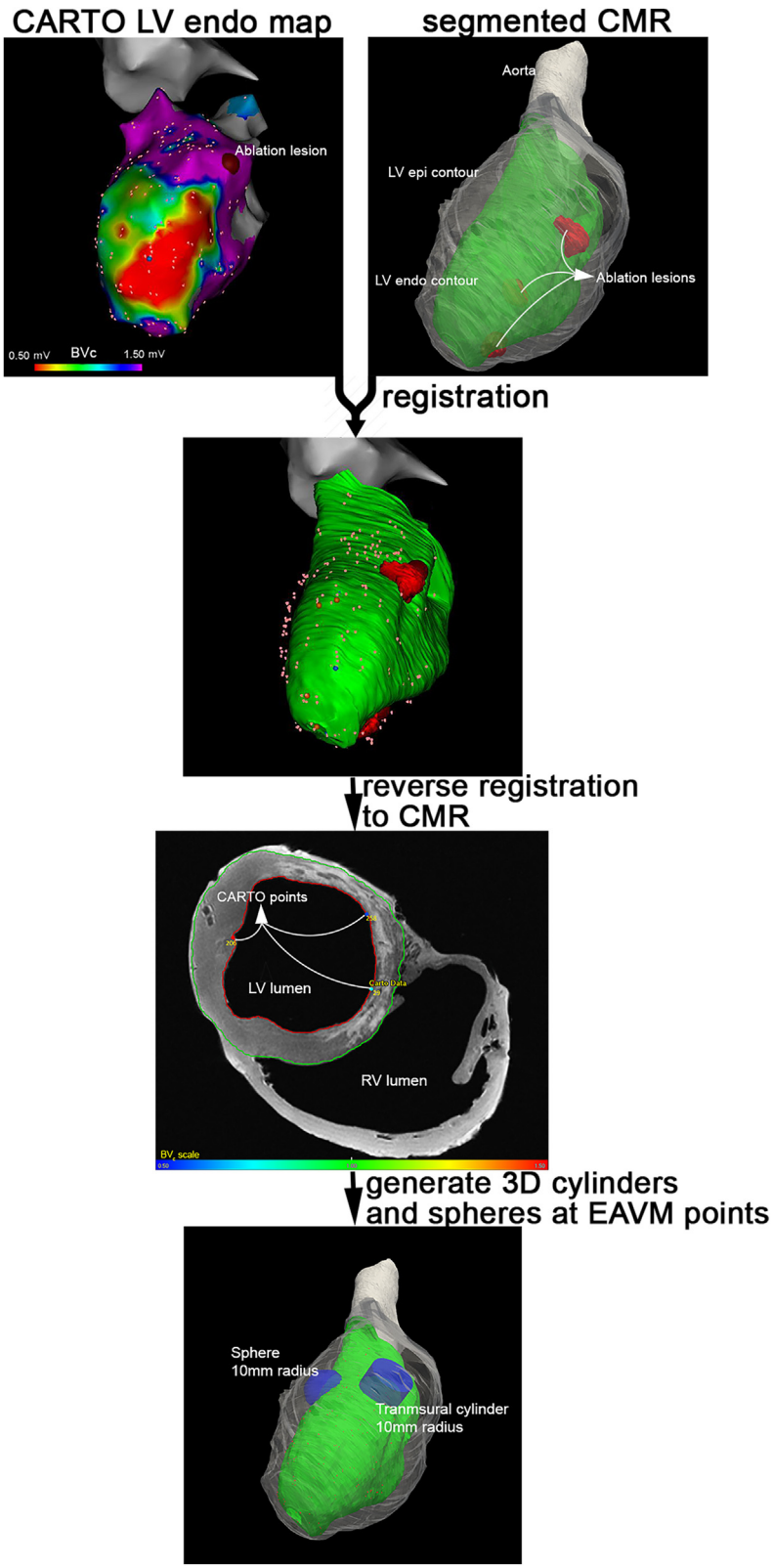

Landmarks used for the merge were the 3 ablation points and the surface registration of left ventricular (LV) and proximal aorta. Examples of a 10-mm radius sphere and transmural cylinder are shown in the bottom panel. 3D = 3-dimensional; CMR = cardiac magnetic resonance; EAVM = electroanatomic voltage-mapping.

FIGURE 4 Example of a Sphere at a CARTO Point

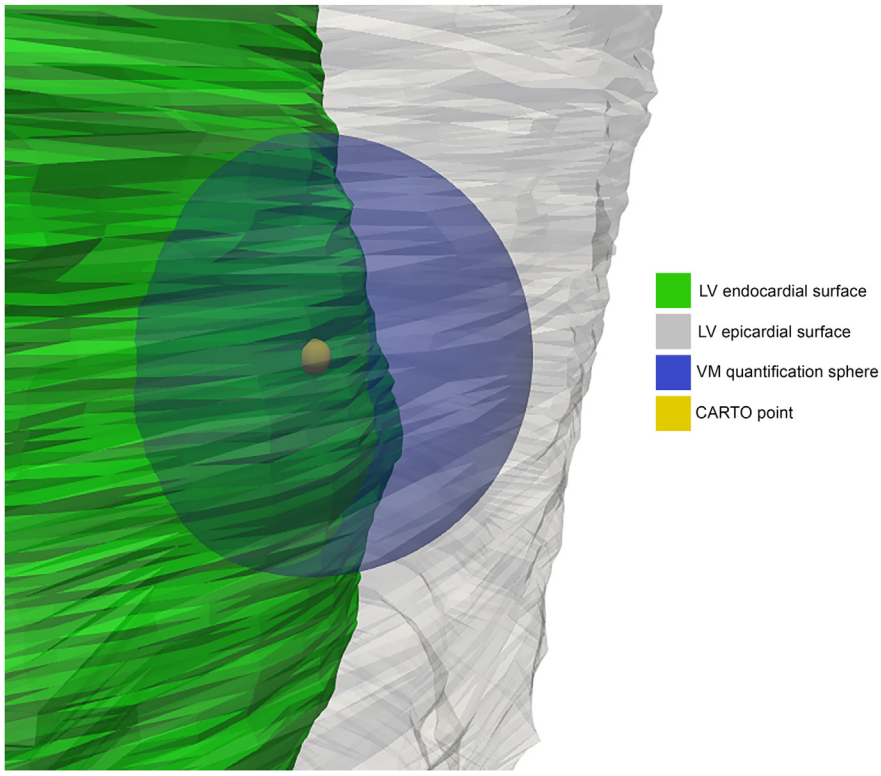

An illustration of a sphere (6-mm radius in this example) centered at an endocardial CARTO point. Within each sphere, the volume of viable myocardium (VM) can be determined. Quantification of VM only occurred between the endocardial and epicardial surface. LV = left ventricular.

and used for the analysis. When analyzing the relationship between UV_{μ} and UV_{c}, and between BV_{μ} and BV_{c}, the simultaneously recorded amplitudes at each location were compared.

After mapping, 3 landmark ablation lesions were placed, distant from the scarred myocardium where possible, for EAVM and LGE-CMR data integration. A ThermoCool SmartTouch SF catheter (Biosense Webster) was used for ablation.

The protocol for in vivo LGE administration, pig sacrifice, and heart extraction has been previously described.[14] A brief description is given in the Supplemental Appendix.

CARDIAC MAGNETIC RESONANCE. The CMR protocol is described in the Supplemental Appendix.

The LGE-CMR stacks were contoured manually on the short axis slices using MASS Research version 2021 (Leiden University Medical Center), creating 3D models that can be exported as .vtk files. Scars were analyzed visually and grouped according to their pattern (**Figure 2**).

VM and scar were subsequently automatically quantified with the binary Otsu method using combined intensity and spatial information, as previously validated and described,[15] and the full-width at half-maximum method (using only core scar).[16] The Otsu method is elaborated on in the Supplemental Appendix.

EAVM INTEGRATION. EAVM were merged with the LGE-CMR model in CARTO (**Figure 3**). If a CARTO point was not already projecting onto the endocardial CMR mesh, it was projected to the nearest point on the CMR surface. At each mapping point, the corresponding CMR WT was measured (**Figure 3**).

The projected EAVM points were categorized as being in or adjacent to the CMR scar area in MASS. Points within a 3-mm radius of any scar on CMR were labelled as scar. Normal voltage cutoffs were defined as the lower fifth percentile of voltages at nonscar CMR points. For comparison, a receiver operating curve (ROC) analysis was also performed to define cutoffs.

TABLE 1 Descriptive LGE-CMR Data of Points in Scar or Nonscar Areas

	Scar (n = 951)	No Scar (n = 1,163)	*P* Value
Wall thickness, mm	5.75 ± 2.05	7.48 ± 2.90	<0.001
VM 3-mm$_{radius}$, mm^3	97.9 (50.2, 167.9)	209.8 (153.9, 272.3)	<0.001
VM 5-mm$_{radius}$, mm^3	285.7 (152.7, 471.6)	582.8 (427.5, 756.3)	<0.001
VM 10-mm$_{radius}$, mm^3	1,275.9 (697.3, 1,909.0)	2,331.1 (1,710.1, 3,025.1)	<0.001

Values are mean ± SD or median (Q1, Q3).
VM = viable myocardium.

COMPARISON BETWEEN LOCAL EAVM AND VIABLE MYOCARDIUM. Endocardial-to-epicardial transmural cylinders were produced within which the VM was quantified in mm^3. Each endocardial CARTO point served as the center of a 3-, 5-, or 10-mm radius cylinder. In addition to transmural cylinders, volumes of VM in subendocardial cylinders of 1 and 3 mm height were also generated for all 3 radii.

In addition to cylinders, multisize spheres were generated at each CARTO point (Figures 3, bottom panel, and 4). The sphere radius R took the integer values between 5 and 15 mm. Within each sphere, the amount of VM was calculated. Both the percentage and the absolute amount of VM (number of pixels) were calculated (Figure 4).

DISTANCE-WEIGHTED VIABLE MYOCARDIUM. In addition to the absolute VM, spherical models incorporating distance-weighting were also evaluated. These models considered that VM closer to the catheter position contributed more toward the measured voltage than remote VM. Two models were used: 1) weighting $1/r$; and 2) weighting $1/r^2$, where r is the distance from the catheter position to the pixel of VM. These 2 weights were used because $1/r^2$ models the decay function of the electric potential of a stationary point dipole, and $1/r$ is the decay function associated with a propagating depolarization front. Due to finite spatial resolution of the LGE-CMR images, the location of the closest voxel to the electrode significantly affects the weighing. Hence, to obtain more robust results, we used a finite cutoff radius Rmin of 3 mm.

TABLE 2 Descriptive Voltage Data of Points in Scar or Nonscar Areas

	Scar (n = 951)	No Scar (n = 1,163)	*P* Value
UV$_c$, mV	4.21 (2.93, 5.96)	6.73 (5.17, 8.46)	<0.001
BV$_c$, mV	1.26 (0.80, 1.89)	2.11 (1.44, 2.97)	<0.001
UV$_\mu$, mV	4.75 (3.38, 6.59)	6.81 (5.27, 8.52)	<0.001
BV$_\mu$, mV	3.04 (1.64, 5.02)	5.40 (3.83, 7.40)	<0.001

Values are median (Q1, Q3).
BV$_c$ = conventional bipolar voltage; BV$_\mu$ = micro bipolar voltage; UV$_c$ = conventional unipolar voltage; UV$_\mu$ = micro unipolar voltage.

STATISTICAL ANALYSIS. Normally distributed data are presented as mean ± SD and non-normally distributed data as median (IQR). Unpaired Student's *t*-tests were used to analyze normally distributed data and Bonferroni corrections added when appropriate. Mann-Whitney *U* test was used for unpaired groups without a normal distribution. Linear correlations were evaluated using Pearson correlation coefficients. A *P* value <0.05 was considered statistically significant. For ROC analyses, the Youden index was used and the area under the curve was given (AUC). R was used (R studio version 1.4.1103, PBC) for statistical analyses.

Voltage outliers were identified using <Q1 - 1.5 IQR and >Q3 + 1.5 IQR. Outliers were reassessed in CARTO (n = 168) and 10 were eventually excluded.

RESULTS

ELECTROANATOMIC MAPPING DATA. A total of 2,322 LV mapping points were collected (220 [Q1, Q3: 216, 260] per swine) (Supplemental Table 1). Of these, 208 were removed because of artefacts (n = 141), premature ventricular contractions (n = 57) and reassessment of outliers (n = 10), giving 2,114 points used in the final analysis. A total of 899 mapping points (43%) had a BV$_c$ <1.5 mV.

CMR SCAR PATTERNS AND DISTRIBUTION. A total of 60 of 153 segments (39%) had any scar, and 93 segments had no scar (61%). All swine had scar in the midanterior, midanteroseptal, and apical-anterior segments. The distribution of affected segments for all swine is provided in Supplemental Figure 1.

Diffuse scar was the most common scar pattern (n = 27, 45%), followed by subendocardial (n = 23, 38%), intramural (n = 6, 10%) and subepicardial scar (n = 4, 7%). Notably, none of the segments had predominantly transmural scar (Figure 2).

With regard to the ablation lesions, the shortest distance between 2 lesions was approximately 40 to 45 mm for each heart. The median distance from the nearest ablation lesions to scar area was 6.45 mm (Q1, Q3: 0, 17.92 mm).

EGM CHARACTERISTICS AND CMR SCARS. A total of 951 EAVM points were located in LGE-CMR-categorized scarred sites and 1,163 in nonscarred LGE-CMR sites. WT at mapping points was reduced in scarred compared with nonscarred sites. Of note, only 4 segments (2.6%) had an average WT of <3 mm (Table 1).

FIGURE 5 Voltages at Scar Points by Wall Thickness

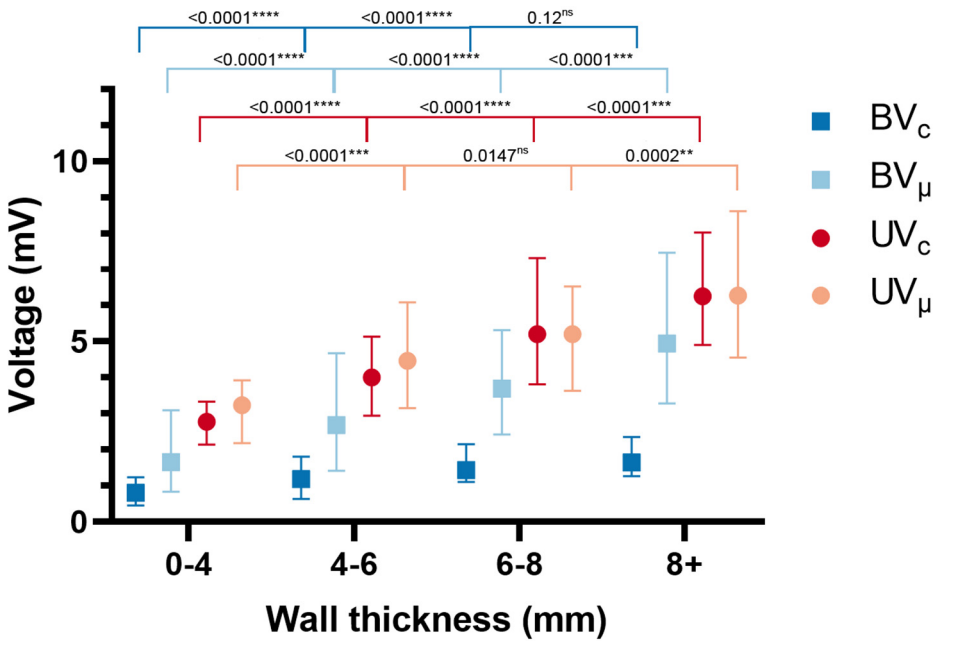

Electroanatomic voltage mapping points (median ± IQR) plotted against local wall thickness at scar points. *P* values are indicated between groups of WT. Asterisks indicate significance levels after Bonferroni correction (*$P \leq 0.05$, **$P \leq 0.01$, ***$P \leq 0.001$, and ****$P \leq 0.0001$ respectively, NS = not significant). Median WT for 8 mm+ category was 8.91 mm (Q1, Q3: 8.27, 9.55 mm).

Recorded voltages at scarred sites were significantly lower compared with the nonscarred sites for all electrodes (Table 2).

Surprisingly, UV_μ and UV_c recorded simultaneously at the same point were similar, and UV_c was not consistently larger or smaller than maximal UV_μ (Supplemental Figure 2). The mean difference between UV_μ and UV_c was only 0.17 ± 2.66 mV. In contrast, BV_μ was consistently larger than BV_c (Supplemental Figure 3). The mean difference between the bipolar voltages was 2.97 ± 2.81 mV.

Based on the fifth percentile of voltages at LGE-CMR nonscarred sites, cutoffs for abnormally reduced voltages were 3.25 mV for UV_c, 0.85 mV for BV_c, 3.50 mV for UV_μ, and 2.01 mV for BV_μ.

Based on the ROC analysis, the best thresholds to distinguish LGE-CMR scarred sites from nonscarred sites were 5.15 mV for UV_c (AUC: 76%), 1.57 mV for BV_c (AUC: 74%), 5.08 mV for UV_μ (AUC: 71%) and 3.53 mV for BV_μ (AUC: 73%).

ASSOCIATION BETWEEN VOLTAGES AND WT. For areas with any scar, all voltages increased with increasing WT across almost the entire range of WT (Figure 5).

Within WT groups, the median UV_μ was only larger than the median UV_c for WT 4 to 6 mm ($P = 0.002$), but was similar for WT <4 and ≥6 mm. In contrast, BV_μ was significantly larger than BV_c within all 4 WT groups ($P < 0.001$).

VM: CYLINDRICAL MODEL. VM was calculated for different cylinder volumes with increasing predefined radii (3, 5, and 10 mm). Figure 6 shows an example of a 5mm radius cylinder in slices through the septal wall, from LV to RV.

All 3 radii gave similar correlations between the volume of VM and all voltage categories (Supplemental Table 2). UV_c had a stronger correlation with VM compared with the other voltage categories.

The VM in 3- and 1-mm subendocardial portions of the transmural cylinder showed no or only a weak correlation to voltage recorded from all electrode recording types (Supplemental Table 2). Of note, BV_μ also showed no relationship with the volume of VM close to the electrodes.

Voltages of all voltage categories increased with an increase in VM volumes within the cylinder from 175 to 350 mm^3, to 350 to 525 mm^3, to >525 mm^3 (the

JACC: CLINICAL ELECTROPHYSIOLOGY VOL. 10, NO. 4, 2024
APRIL 2024:637–650

FIGURE 6 Example of a Viable Myocardium Cylinder With a 5-mm Radius Shown on the LGE-CMR

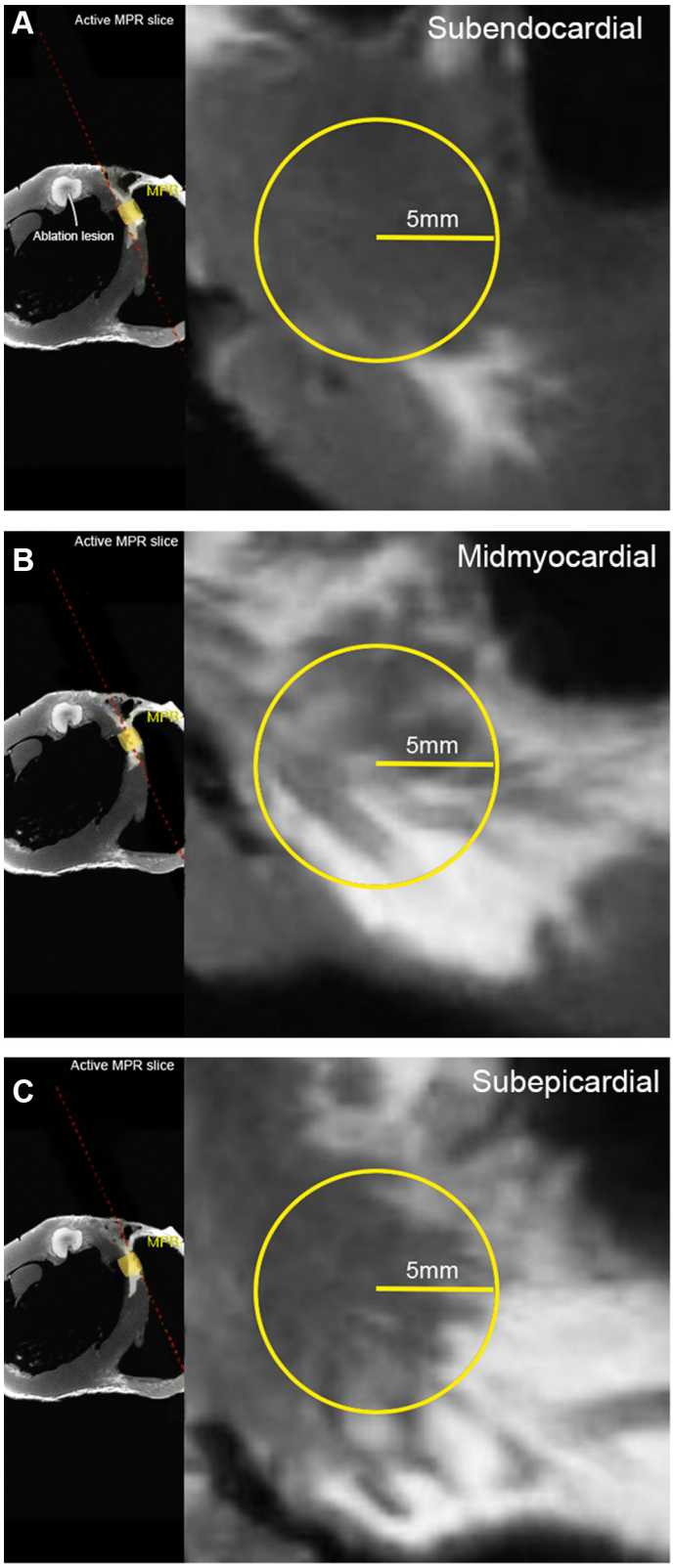

Continued on the next page

latter is equivalent to a cylinder with height >6.69 mm) (Figure 7). Of note, the voltages for the 4 voltage categories were similar for cylinders with the low VM volume categories of 0 to 175 and 175 to 350 mm^3 (Figure 7).

Within VM groups, the voltage values for UV_μ were statistically comparable to UV_c, reaching a significant difference only for VM group 175 to 350 mm^3 ($P = 0.017$). There was no significant difference between unipolar voltages in the remaining VM groups. In contrast, BV_μ was significantly larger than BV_c within all 4 VM groups ($P < 0.001$).

VM: SPHERICAL MODEL, WITH DISTANCE-WEIGHTING. Figure 8 shows the correlation between the peak-to-peak amplitude of unipolar signals and the amount of VM in a sphere of radius R around the electrode. The correlation improves up to the radii of 10 mm (for UV_c) and 8 mm (for UV_μ) and is then flat despite the inclusion of more distant portions of myocardium. The unipolar amplitude correlated better with the absolute amount of VM than the percentage. For radii larger than 12 mm, the distance-weighted quantities score slightly better and the unweighted correlation saturates and decreases for the UV_c. In the case of UV_μ, the unweighted correlation drops more sharply after saturation. In general, the UV_c has a slightly greater correlation than the UV_μ (Figure 8).

DISCUSSION

MAIN FINDINGS. To the authors' knowledge, this is the first study to perform a direct comparison of UV and BV recorded from conventional and narrow-spaced small electrodes from endocardial regions overlying variable *volumes* of VM to determine the "field-of-view" for voltage mapping. Ex vivo high-resolution LGE-CMR was utilized in a reperfusion swine infarct model to permit accurate delineation of VM.

Important findings are as follows:

1. Multiple scar patterns were observed in the very early-reperfusion ischemic swine model using ex vivo high-resolution LGE-CMR that differ from the scar distribution pattern seen in prior early reperfusion and chronic occlusion infarct models: diffuse (45%), intramural (10%), and subepicardial (6.7%) scar, whereas no segment showed predominantly confluent transmural scar.
2. Surprisingly, UV from conventional and microelectrodes recorded simultaneously at the same site did not differ. As a consequence, voltage cutoffs, defined as the lower fifth percentile of voltages at non-scar LGE-CMR points, were similar for

UV_c and UV_μ (3.25 and 3.50 mV, respectively). In contrast bipolar voltages from micro electrodes (BV_μ) were greater than those of conventional electrodes (BV_c) (2.01 mV vs 0.85 mV, respectively).

3. Increasing volumes of VM within transmural cylinders of different radii, up to a 10-mm radius, correlated with increasing voltage for all electrode recording types.
4. Neither conventional nor microelectrodes recordings could distinguish between low (<350 mm^3) and very low (<150 mm^3) amounts of transmural VM (**Central Illustration**).
5. The correlation of UV_c and UV_μ with VM improves with increasing radii for VM quantitation out to a radius of 10 mm for UV_c and 8 mm for UV_μ, and not beyond, suggesting that the effective field-of-view for unipolar recordings does not extend beyond those distances (**Central Illustration**). Microelectrodes are expected to have a smaller field-of-view compared with conventional, large tip electrodes. For unipolar recordings, however, this difference is surprisingly small. VM within a radius of approximately 8 mm will still affect local EGM amplitudes recorded with microelectrodes. For large electrodes, this radius of influence is approximately 10 mm.

SCAR PATTERN AND QUANTIFICATION OF VIABLE MYOCARDIUM IN EARLY REPERFUSION INFARCTS. In this early-reperfusion swine model, 62% of affected segments showed diffuse, midmyocardial, or subepicardial scar distribution with limited wall thinning. This is remarkably different from the chronic occlusion infarct models. Of note, diffuse fibrosis and midmyocardial scar is often observed in nonischemic cardiomyopathy.[17-21] Our reperfusion infarct model, which may mimic human reperfusion and also nonischemic scars, may be valuable to evaluate the performance of various catheters, electrode sizes and configurations.

Leshem et al[9] have also used a porcine model of temporary but longer LAD occlusion (180 minutes). They found, on LGE-CMR, that approximately one-third of LGE visualized scar volume was distributed subendocardially, but they also described transmural scars. The lack of such confluent transmural scar in our study may be explained by the shorter LAD occlusion time.

Voltage mapping to delineate scar has been mainly validated in a chronic occlusion porcine infarct model resulting in dense transmural scars with wall thinning.[7] Data validating voltage mapping and the performance of conventional- and narrow-spaced microelectrodes, for the estimation and localization of VM for diffuse, nontransmural, midmyocardial, and subepicardial scar patterns in particular if WT is preserved, are limited.

QUANTIFICATION OF VM: A NOVEL APPROACH. For this purpose, we have proposed a new method to quantify VM for any myocardial volume at any mapping location based on in vivo LGE administration and ex vivo high-resolution LGE-CMR. This method is different from all prior studies which have compared mapping data with VM on a 2D slice, either side-by-side or after integration of data sets.[9,13,21]

The true field-of-view, ie, the extent and distance of VM contributing to the recorded voltages at 1 site, for all electrodes is unknown. This information is particularly important if endocardial voltage mapping is used to delineate midmyocardial and subepicardial fibrosis in nonischemic cardiomyopathies. Thus, we have investigated the relation between VM and UV and BV recorded from different size electrodes for different volumes of VM surrounding the endocardial catheter position.

VOLTAGE CUTOFF VALUES. Of note, if recorded simultaneously at the same site and during the same beat, UV_c and UV_μ were similar with a mean difference of only 0.17 mV. As a consequence, the UV_c and UV_μ cutoffs based on the fifth percentile barely differed (3.25 and 3.50 mV, respectively). Because UV are the recorded voltages, this data supports a comparable field-of-view for the 3.5-mm tip electrode and the microelectrodes. In contrast, the bipolar EGM is constructed by summing the inverted unipolar EGM recorded from a second electrode thereby eliminating those far field components that are recorded from both electrodes. If recorded from the same position and the same beat, the largest of the 3 BV_μ was significantly larger than the BV_c. Consequentially, the BV_μ and BV_c cutoffs were further apart (2.01 and 0.85 mV, respectively). These data strongly advocate catheter- and electrode-specific voltage cutoff values and electrode configurations that compensate for the angle of incidence and wave front directionality.

FIGURE 6 Continued

On the left, the short-axis view is shown with the perpendicular multiplanar reformation (MPR) lines through the septal scar and through the transmural cylinder in yellow. The red line indicates the active slice shown on the corresponding panel on the right side. (A) The yellow circle, indicating the pixels used for viable myocardium calculation, is projected on the LV endocardium. The circle (which is a transmural cylinder in 3-dimensions) has a CARTO point at the center. (B) Midmyocardial myocardium. (C) Subepicardial myocardium, nearing the right ventricle.

FIGURE 7 VM Against Voltages for Scar Points

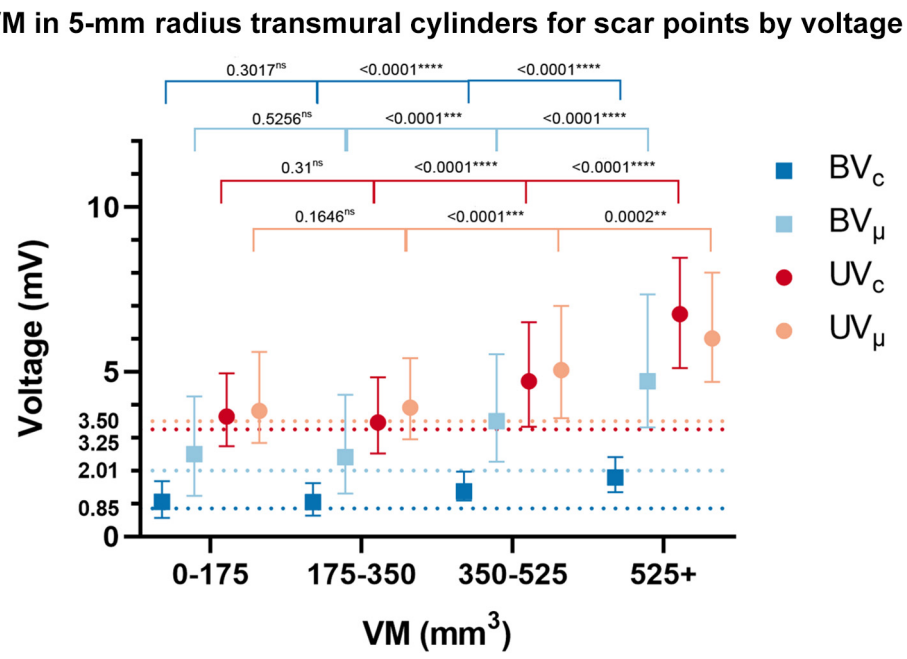

Voltages (median ± IQR) plotted against viable myocardium (VM) (groups resemble quartiles) in 5-mm radius transmural cylinders at scar points. The dashed lines indicate the voltage cut off for abnormal reduction of VM based on the 5% percentile. *P* values are indicated between groups of VM. Asterisks indicate significance levels after Bonferroni correction. *$P \leq 0.05$, **$P \leq 0.01$, ***$P \leq 0.001$, and ****$P \leq 0.0001$. NS = not significant.

The voltage cutoffs in our data vary considerably from those in the study by Leshem et al.[9] Their fifth percentile cutoffs were: UV_c 4.1 mV (vs 3.25 mV), UV_μ 2.9 mV (3.5 mV), BV_c 1.19 mV (0.85 mV), and BV_μ 1.3 mV (2.01 mV), respectively.

A general limitation of the fifth percentile cutoff method is a potential sampling bias. For instance, more mapping points around the valve areas may lead to a lower cutoff because the fibrous tissue influences the recorded voltage. Additionally, Leshem et al[9] used healthy pigs to extrapolate cutoff voltage values, in contrast to our study where nonscarred remote myocardium served as a reference. Moreover, the LAD occlusion in our study was only 65 minutes, and remote remodeling was considered minimal based on the absence of abnormal fibrosis in transmural biopsies taken from remote myocardium in a prior study.[13] Depending on the field-of-view the reduction of VM in the infarcted area or close to valve annuli can influence UV at remote sites. Of importance, clinically applied voltage mapping aims to identify affected areas within the chamber, and it seems reasonable to use cutoff values that are derived from nonaffected myocardium in an infarct model, rather using healthy subjects.

FIELD-OF-VIEW. Comparison of voltages with WT. Prior studies from our group comparing voltage mapping with 2D histology in the infarct pig model and in humans with DCM have shown a linear relationship between voltages and WT.[13,21] The study confirms and extends the finding of a positive correlation between recorded UV and BV and increasing WT for conventional and microelectrodes, including UV_μ.

COMPARISON OF VOLTAGES WITH 3D VOLUMES OF VIABLE MYOCARDIUM. Multiple findings from this nontransmural scar model study argue that microelectrodes in the studied configuration are affected by surrounding VM in terms of width, and in terms of depth, up to a distance of approximately 8 mm (10 mm for conventional electrodes). More distant VM does not appear to contribute further toward voltage. Thus, microelectrodes just minimally limit the field-of-view for unipolar recordings. The idea of comparable fields of view is also supported by the fact that UV_c and UV_μ amplitudes were very similar at each CARTO point, whereas the derived BV_c and BV_μ amplitude differences were much larger. This important far-field influence likely hampers the

FIGURE 8 **Determining the Field of View, Modeled as a Sphere**

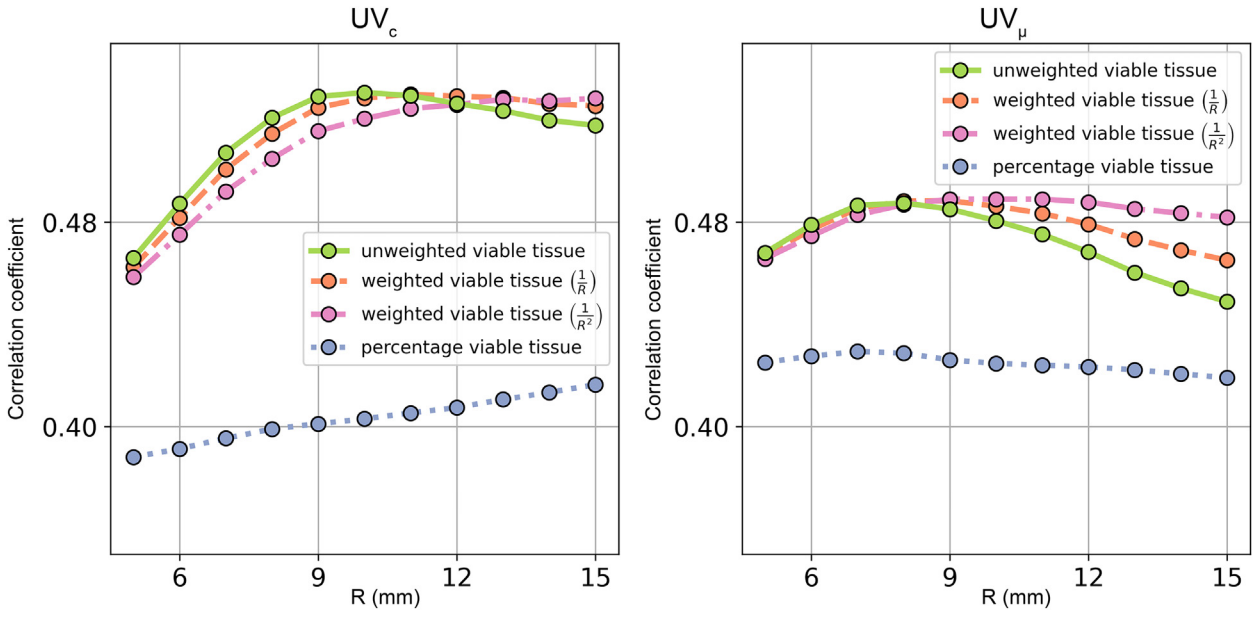

The Pearson's r correlation coefficient as a function of the sphere radius R for the conventional unipolar voltage (UV_c) (left) and micro unipolar voltage (UV_μ) (right). Sphere size was adjusted in 1-mm intervals. Effect of distance weighting and percentage of viable myocardium is shown.

ability to accurately detect subendocardial viable layers by VM and may also challenge using cutoff voltage values to detect viable channels within reperfused ischemic and likely also within non-ischemic scars.

The slightly lower correlation between voltage and VM for UV_μ compared with UV_c is likely caused by the smaller area of the microelectrodes that makes them more sensitive to local spatial variations of the potential.

The fraction of VM to WT or volume appears to be an inferior metric for judging VM compared with absolute mass quantification.

For the conclusions regarding field-of-view, we mainly relied on unipolar voltage analysis because unipolar voltages are simpler to interpret. This is because they are not influenced by factors such as direction of wave front propagation, angle of incidence, and interelectrode distance. We also mainly relied on volume of VM rather than WT because the 3D parameter is a more accurate representation of VM.

BENEFIT OF MICROELECTRODES. From this data, it appears that the main benefit of the 3 microelectrodes lies in their perpendicular orientation relative to the conventional electrodes and in the 3 different angles, activated with temporal delay. This permits a BV reading in 3 directions in another plane, such that EGM detection is robust in areas with anisotropic conduction, and partially explains higher BV values despite similar UV amplitudes. The reduced cancellation results in larger BV_μ amplitudes with a better signal-to-noise ratio and produces a sharper BV_μ EGM that can reveal fractionation and small late potentials not easily detected by conventional electrodes.[9,13] Indeed, prior studies have shown that endocardial mapping with microelectrodes have added benefits for recognizing a thin subendocardial layer of surviving viable layer overlying otherwise transmural scar.[9,12]

DISTANCE WEIGHTING. As the amplitude of an EGM generated by activity in a myocardial bundle is inversely proportional to the square of the distance between the myocardial bundle and the recording site for UV, remote myocardium contributes less to EGM voltage.[21] Hence, the distance-weighted UV may better correlate with the amount of VM. Indeed, at larger sphere radii, $^1/_{r^2}$-weighting seems to outperform $^1/_r$, which in turn outperforms unweighted VM. At smaller radii, the opposite seems true. This could

JACC: CLINICAL ELECTROPHYSIOLOGY VOL. 10, NO. 4, 2024
APRIL 2024:637-650

CENTRAL ILLUSTRATION Voltage and Volume of Viable Myocardium

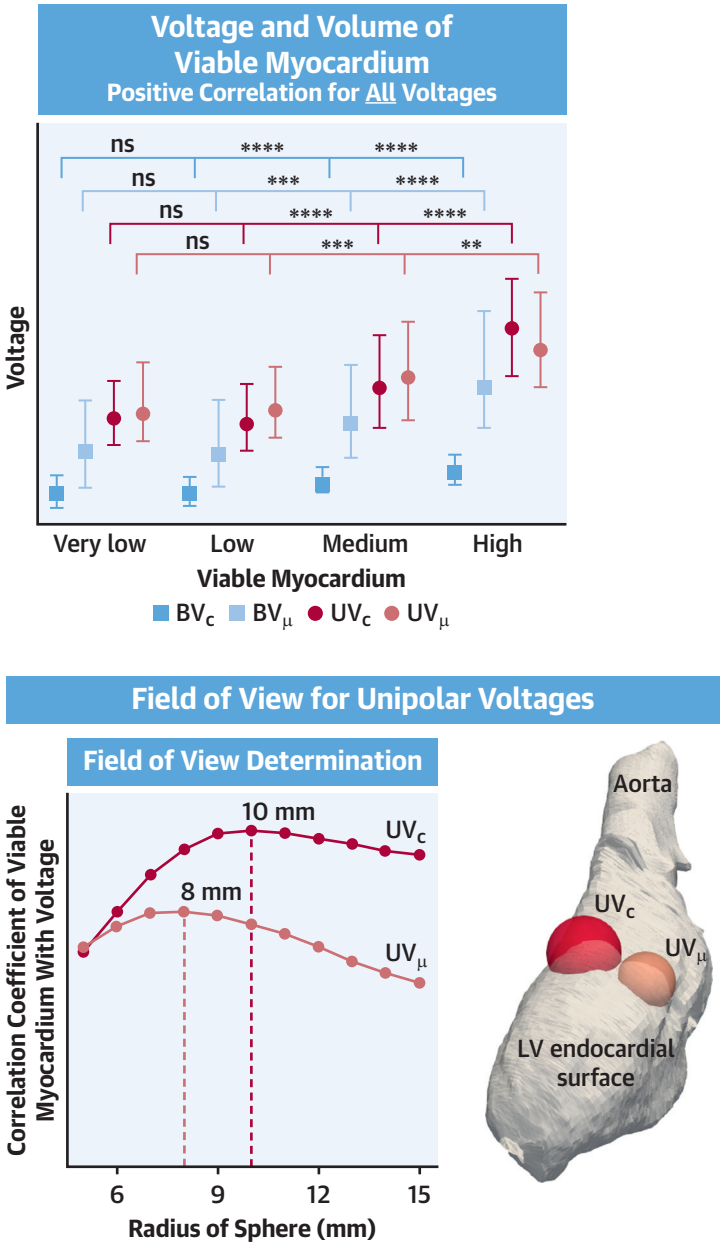

Omara S, et al. J Am Coll Cardiol EP. 2024;10(4):637-650.

(Top) Relationship between voltages (from conventional electrodes [unipolar voltage (UV_c) and bipolar voltage (BV_c)] and microelectrodes [unipolar (UV_μ) and bipolar voltage (BV_μ)]) and *volume* of viable myocardium (VM) generated as a transmural cylinder with a radius of 5 mm. All 4 voltages are influenced by remote VM, yet cannot distinguish between low and very low volumes of VM. (Bottom) VM beyond a 10-mm sphere does not influence UV_c amplitude, and beyond 8-mm sphere does not influence UV_μ amplitude. NS = not significant.

be explained by a slight mismatch between the EAVM and CMR registration. Thus, we conclude that $^1/_{r^2}$ appears to be the best scaling but that the inevitable registration mismatch limits predictive power at short distances. We are currently exploring the influence of distance weighting using mathematical modelling, where wave front propagation will be incorporated because this impacts bipolar voltages.

STUDY LIMITATIONS. Although we used a technique that aimed to preserve the myocardial geometry until after the ex vivo LGE-CMR, some contraction of the tissue may have occurred. This can reduce the correlation values because it can introduce discrepancy between the 3D CARTO LV map and the 3D CMR LV mesh. The ablation lesions that were made to facilitate the merge meant that underlying scar from the induced MI was no longer visible on LGE-CMR images and that these volumes had to be identified as VM. These were relatively small lesions; thus, the effect on correlation is likely to be almost negligible.

Orientation of wave front propagation was not included in our current model. This may limit the interpretation of bipolar voltage amplitudes with respect to viable myocardium.

CONCLUSIONS

Myocardial infarction treated with reperfusion is characterized by a nontransmural scar and a myriad of scar patterns that can resemble nonischemic cardiomyopathies. Simple voltage cutoff values for scar detection are simplistic and reflect the potential arrhythmia substrate in a limited way because WT and the transmural volume of VM have a significant impact on EGM amplitude for both conventional and microelectrodes. VM is limited in defining heterogeneous tissue with low amounts of VM and neither conventional nor microelectrodes can distinguish thin from thick areas of subendocardial VM. The field-of-view for unipolar recordings appears to be 8 to 10 mm, and is relatively similar for small- and large-tip electrodes. The observed field-of-view can explain the inability of voltage mapping to delineate subendocardial areas with low amounts of VM in the reperfused infarct model without transmural scars. The findings further contribute to our understanding and ability to interpret voltage maps.

FUNDING SUPPORT AND AUTHOR DISCLOSURES

This study was partially supported by an investigator-initiated grant from Biosense Webster (a Johnson and Johnson company). Dr Tofig has received research support from the Arvid Nilssons Foundation. Mr Leenknegt was funded by FWO-Flanders grant number G025820N and KU Leuven grant STG/19/007. Outside this work, Dr Nielsen has received research support from the Novo Nordisk Foundation (grants NNF16OC0018658 and NNF17OC0029148). Dr Lukac has received an institutional grant from Abbott Denmark and Biosense Webster. All other authors have reported that they have no relationships to disclose that are relevant to the contents of this paper.

ADDRESS FOR CORRESPONDENCE: Dr Katja Zeppenfeld, Department of Cardiology, Leiden University Medical Centre, P.O. Box 9600, 2300 RC Leiden, the Netherlands. E-mail: k.zeppenfeld@lumc.nl.

PERSPECTIVES

COMPETENCY IN MEDICAL KNOWLEDGE 1: For unipolar voltage mapping, the field-of-view of conventional and microelectrodes is similar and appears to be limited to a 10- and 8-mm sphere, respectively. VM is unlikely to provide meaningful information for more remote arrhythmia substrates.

COMPETENCY IN MEDICAL KNOWLEDGE 2: Voltage cutoffs are not reliable in delineating nontransmural scar. Rather, amplitudes are significantly influenced by WT and the transmural volume of viable myocardium for both conventional and microelectrodes.

COMPETENCY IN MEDICAL KNOWLEDGE 3: Early reperfusion MI can lead to fibrosis patterns that resemble nonischemic cardiomyopathy.

TRANSLATIONAL OUTLOOK: Another study aimed at determining the field of view for bipolar VM would further add to our understanding of EAVMs. This would need to incorporate additional variables such as wave front direction.

REFERENCES

1. De Bakker JM, Van Capelle FJ, Janse MJ, et al. Slow conduction in the infarcted human heart. 'Zigzag' course of activation. *Circulation*. 1993;88(3):915-926.

2. De Bakker JM, Van Capelle FJ, Janse MJ, et al. Reentry as a cause of ventricular tachycardia in patients with chronic ischemic heart disease: electrophysiologic and anatomic correlation. *Circulation*. 1988;77(3):589-606.

3. Dillon SM, Allessie MA, Ursell PC, Wit AL. Influences of anisotropic tissue structure on reentrant circuits in the epicardial border zone of subacute canine infarcts. *Circ Res*. 1988;63(1):182-206.

4. De Bakker JMT, Coronel R, Tasseron S, et al. Ventricular tachycardia in the infarcted, Langendorff-perfused human heart: Role of the arrangement of surviving cardiac fibers. *J Am Coll Cardiol*. 1990;15(7):1594-1607.

5. Ono S, Waldman LK, Yamashita H, Covell JW, Ross J. Effect of coronary artery reperfusion on transmural myocardial remodeling in dogs. *Circulation*. 1995;91(4):1143-1153.

6. Reimer KA, Jennings RB. The "wavefront phenomenon" of myocardial ischemic cell death. II. Transmural progression of necrosis within the framework of ischemic bed size (myocardium at risk) and collateral flow. *Lab Invest*. 1979;40(6):633-644.

7. Wrobleski D, Houghtaling C, Josephson ME, Ruskin JN, Reddy VY. Use of electrogram characteristics during sinus rhythm to delineate the endocardial scar in a porcine model of healed myocardial infarction. *J Cardiovasc Electrophysiol*. 2003;14(5):524-529.

8. Sramko M, Hoogendoorn JC, Glashan CA, Zeppenfeld K. Advancement in cardiac imaging for treatment of ventricular arrhythmias in structural heart disease. *Europace*. 2019;21(3):383-403.

9. Leshem E, Tschabrunn CM, Jang J, et al. High-resolution mapping of ventricular scar: evaluation of a novel integrated multielectrode mapping and

ablation catheter. *J Am Coll Cardiol EP*. 2017;3(3):220–231.

10. Berte B, Zeppenfeld K, Tung R. Impact of micro-, mini- and multi-electrode mapping on ventricular substrate characterisation. *Arrhythm Electrophysiol Rev*. 2020;9(3):128–135.

11. Barkagan M, Sroubek J, Shapira-Daniels A, et al. A novel multielectrode catheter for high-density ventricular mapping: electrogram characterization and utility for scar mapping. *EP Europace*. 2020;22(3):440–449.

12. Tschabrunn CM, Roujol S, Dorman NC, Nezafat R, Josephson ME, Anter E. High-resolution mapping of ventricular scar. *Circ Arrhythm Electrophysiol*. 2016;9(6):e003841.

13. Glashan CA, Tofig BJ, Tao Q, et al. Multisize electrodes for substrate identification in ischemic cardiomyopathy: validation by integration of whole heart histology. *J Am Coll Cardiol EP*. 2019;5(10):1130–1140.

14. Glashan CA, Tofig BJ, Tao Q, et al. Whole heart histology: a method for the direct integration of histology with electrophysiological and imaging data. *J Am Coll Cardiol EP*. 2020;6(4):461–462.

15. Tao Q, Milles J, Zeppenfeld K, et al. Automated segmentation of myocardial scar in late enhancement MRI using combined intensity and spatial information. *Mag Res Med*. 2010;64(2):586–594.

16. Roes SD, Borleffs CJW, Geest RJvd, et al. Infarct tissue heterogeneity assessed with contrast-enhanced MRI predicts spontaneous ventricular arrhythmia in patients with ischemic cardiomyopathy and implantable cardioverter-defibrillator. *Circ Cardiovasc Imaging*. 2009;2(3):183–190.

17. de Leeuw N, Ruiter DJ, Balk AH, de Jonge N, Melchers WJ, Galama JM. Histopathologic findings in explanted heart tissue from patients with end-stage idiopathic dilated cardiomyopathy. *Transpl Int*. 2001;14(5):299–306.

18. Haqqani HM, Tschabrunn CM, Tzou WS, et al. Isolated septal substrate for ventricular tachycardia in nonischemic dilated cardiomyopathy: incidence, characterization, and implications. *Heart Rhythm*. 2011;8(8):1169–1176.

19. Nakahara S, Tung R, Ramirez RJ, et al. Characterization of the arrhythmogenic substrate in ischemic and nonischemic cardiomyopathy implications for catheter ablation of hemodynamically unstable ventricular tachycardia. *J Am Coll Cardiol*. 2010;55(21):2355–2365.

20. Soejima K, Stevenson WG, Sapp JL, Selwyn AP, Couper G, Epstein LM. Endocardial and epicardial radiofrequency ablation of ventricular tachycardia associated with dilated cardiomyopathy: the importance of low-voltage scars. *J Am Coll Cardiol*. 2004;43(10):1834–1842.

21. Glashan CA, Androulakis AFA, Tao Q, et al. Whole human heart histology to validate electroanatomical voltage mapping in patients with non-ischaemic cardiomyopathy and ventricular tachycardia. *Eur Heart J*. 2018;39(31):2867–2875.

KEY WORDS late-gadolinium enhancement, microelectrodes, non-transmural scar, voltage mapping

APPENDIX For expanded Methods and Results sections as well as supplemental tables and figures, please see the online version of this paper.